A comparative study of cell behavior on different energetic and bioactive polymeric surfaces made from elastin-like recombinamers

Carmen García-Arévalo,[ab] María Pierna,[ab] Alessandra Girotti,[ab] Francisco Javier Arias[ab] and José Carlos Rodríguez-Cabello*[ab]

This work explores cell behavior as a function of the topographic (fibers *vs.* films) and bioactive (RGD inclusion) design of multifunctional surfaces obtained from elastin-like recombinamers (ELRs). The surfaces have been analyzed for their differential roughness, wettability, and surface free-energy, as their precise contribution and importance of controlling critical aspects of cell behavior were investigated. The results suggest that the highest proliferative capacity of cells on the highly hydrophilic surfaces is more closely related to the surface properties than to the presence of adhesion sequences, although they act as an accelerating factor. However, on energetically unfavorable surfaces, bioactivity acquires decisive significance in ensuring cell adhesion and proliferation.

Introduction

As most biological reactions occur either on surfaces or at interfaces, the surface quality plays a significant role in the development of biomaterials and medical devices in which precise control of the interaction between material surfaces and the biological environment is required.[1,2] The control of bio-interfacial phenomena is an important but elusive goal that affects the development of materials capable of promoting substantial adhesion and cell proliferation. This is especially true for new generation biomaterial surfaces, where conventional parameters such as surface energy and hydrophobicity converge with more sophisticated properties such as nanostructuration and the presence of specific bioactivities. In these cases, the interaction between classical functionalities and novel ones results in complex systems where the existence of synergies or mutual interference can play a significant role.

It is well known that cell function is modulated by the spatial organization of their substrates on sub-millimetre[3] and sub-micrometre[4] scales. However, the emergence of nanotechnologies now opens up numerous possibilities for the application of nanosized features from a wide variety of extracellular matrix (ECM) molecules. Thus, for example, collagen, elastin, and keratin, which are often used in biomaterials and for surface modulation, have been shown to improve biocompatible responses and result in better tissue integration of medical implants when they comply with the nanoscale features of the natural microenvironment of cells.[5–7]

One of the physicochemical methodologies that has been proposed for the manufacture of cellular scaffolds and for modifying the chemical and topographic features of different substrates involves the use of fibrous components that mimic the ECM structure of natural tissues.[8] In this respect, nanofibers have been used as scaffolds for musculoskeletal (including bone, cartilage, ligament, and skeletal muscle), skin, vascular, and neural tissue engineering, and as carriers for the controlled delivery of drugs, proteins, and DNA.[9] Electrospinning has gained widespread interest as a polymer processing technique due to its relative ease of use, adaptability, and the possibility to engineer scaffolds with a desired micro- to nanoscale topography and high porosity.[10]

Elastin is an insoluble elastic protein that predominates in those tissues where elasticity is of major importance (skin, arteries, lungs, ligament, and specialized cartilages), imparting elasticity and resilience. Despite the benefits of using human elastin in the manufacture of scaffolds,[11] its high insolubility has limited its utility to researchers. However, the increasing availability of recombinant forms of elastin-inspired polypeptides, recently renamed as "elastin-like recombinamers" (ELRs),[12] has allowed the formation of a wide range of biomaterial-based constructs and composites that benefit from elastin's ability to self-assemble and elasticity,[13] such as aggregates,[14] films,[15,16] fibers,[17] micelles,[18] nanoparticles,[19] and hydrogels,[20] either alone or as hybrid systems, in a wide range of sizes, morphologies, and functional possibilities.

Since the first report of Huang *et al.*[21] on fiber formation from an elastin analogue, most reports concerning its potential use in the production of elastin fibers have tended to focus on their physical characterization, with much less attention being paid to cellular aspects.[17,21,22] As a general trend in the literature, the study of the influence of different topographies and bioactivities

on cell behavior has been carried out following a highly reductionist approach. Indeed, the current tendency is to study these parameters in an isolated and independent fashion.[23,24] However, this means that the potential existence of synergies or hindrances amongst the conceptually different functions present in the surface material and their relative influence on cell behavior remain mainly unexplored for the majority of novel complex and multifunctional materials.

This work aims to perform a comparative analysis of the precise contribution and importance of two different topographies, namely fibers and films, on cell behavior and to contrast them with topographically identical substrates bearing a bioactive function. To this end, an extensive characterization of the surfaces has been undertaken in order to gain a better understanding of their physicochemical properties and functionality, especially their roughness, wettability, and the related concepts of surface free-energy (SFE) and interfacial free-energy (IFE).

Experimental

ELR biosynthesis and characterization

The gene polymerization techniques, cloning and molecular biology procedures, ELR biosynthesis in *Escherichia coli* expression systems, and purification protocols have been described in detail previously.[15,25–27]

Molecular characterization of the recombinamers used in this work was routinely carried out by sodium dodecyl sulfate polyacrylamide gel electrophoresis (SDS-PAGE), matrix-assisted laser desorption/ionization time-of-flight (MALDI-TOF) mass spectroscopy (MS), amino-acid composition determination, nuclear magnetic resonance (NMR) spectroscopy, and differential scanning calorimetry (DSC). All techniques confirmed the correctness of the final composition of the recombinamers used. The transition temperatures determined by DSC, and the theoretical and experimental molecular weights (M_w) obtained from MALDI-TOF are provided in Table 1.

Topographical design of ELR-based surfaces

Synthesis of electrospun ELR-based nanofibers. Aqueous ELR solutions (25% (w/w), pH 7.4) were used during the electrospinning process. These solutions were infused through an 18 G × 1″ needle at a constant flow rate of 0.25 mL h^{-1} and a voltage of between 38 and 40 kV, as determined from previous optimization studies. Recombinamer fibers were directed to a grounded, circular, indium tin oxide (ITO) collector with a diameter of 12 mm over a collector distance of 15 cm. Electrospun surfaces were cross-linked by immersion in 10% HMDI/acetone solution overnight and then exhaustively washed with ultrapure deionized water.

Table 1 Results of MALDI-TOF MS analysis, the transition temperatures obtained by DSC, and final yields of the recombinamers

ELR	Theoretical M_w/Da	Experimental $M_w \pm$ SD/Da	T_t/°C	Yield/ mg L^{-1}
IK24	51 980	51 996.5 ± 11.3	31.5	540
RGD6	60 661	60 542.5 ± 10.8	31.1	286

Synthesis of ELR-based films. Aqueous ELR solutions (50 mg mL^{-1}, pH 7.4) were deposited on circular cover glasses (diameter: 12 mm; Thermo Scientific). After solvent evaporation by incubation for 8 h at 60 °C, the dry films were cross-linked by immersion in 10% HMDI/acetone solution overnight and then exhaustively washed with ultrapure deionized water.

Sterilization of ELR-based surfaces. Both ELR surfaces used in cell culture were sterilized by immersion in 70% ethanol for 30 minutes then exhaustively rinsed with 0.1% PBS/Bovine Serum Albumin (BSA) followed by washing with 0.1% Dulbecco's Modified Eagle's Medium (DMEM)/BSA.

Surface characterization

Scanning Electron Microscopy (SEM). Surfaces completely covered with recombinamers were observed by SEM using an FEI Quanta 200 FEG instrument in low vacuum mode. SEM images were used to determine the fiber diameter and thickness and to check the surface homogeneity. Fiber diameters were determined by counting 100 independent fibers using *ImageJ* software.

Atomic Force Microscopy (AFM). AFM measurements were performed using a Dimension 3100 microscope controlled by a Nanoscope IV controller system (Digital Instruments) in tapping mode using V-shaped Si3N4 tips (OMCL TR400PSA, Olympus, Japan). AFM images were taken from PBS immersed samples, with a nominal spring constant of 0.32 N m^{-1}. The scan area was 10 μm × 10 μm and the root-mean-square (RMS) roughness of the surfaces was evaluated for regions of 5 μm × 5 μm.

Surface roughness quantifies the vertical variations of a real surface from its ideal form. One of the most common parameters used to describe the degree of roughness of a surface is the root mean square (RMS) roughness, which is defined as (eqn (1)):

$$Rq = \sqrt{\frac{1}{n}\sum_{i=1}^{n} y_i^2} \quad (1)$$

where "n" corresponds to the total number of pixels in the image and "i" corresponds to the number of individual pixels. This parameter is especially useful when these variations in Z height are positive and negative from the ideal mean line.

Five randomized sections from three different surfaces were created for each image to determine the surface roughness of the polymeric surfaces.

X-Ray photoemission spectroscopy (XPS). XPS surface analysis was used to monitor the modifications produced in the outermost (1–10 nm) layers of the surfaces. XPS experiments were carried out using a Physical Electronics (PHI) 5500 spectrometer equipped with a monochromatic X-ray source (Al Kα line with an energy of 1486.6 eV and 350 W). The pressure inside the analysis chamber was 10^{-7} Pa. All measurements were performed at an angle of 45° with respect to both the X-ray source and analyzer. Survey scans were taken in the range 0–1100 eV and high resolution scans were obtained for the C1s, N1s, and O1s peaks. The elemental surface composition was estimated from the area of the different photoemission peaks taken from

the survey scans modified by their corresponding sensitivity factors.

Contact angle measurements. Hood dried samples were placed onto the platform surface of a Data Physics OCA20 system instrument. The drop profile images for the advancing and receding drops during micro-syringe dispensation were recorded using an adapted CCD video camera. The three-phase contact line of the liquid drop was made to advance or retreat by adding or withdrawing the liquid and the advancing and receding contact angles were measured in the stable phase of advance or recoil on both sides of the drop (the average values are reported). The stainless-steel needle tip was always kept at the top of the sessile drop and immersion of the needle into the drop was avoided during the measurements to prevent distortion of the drop shape by the needle.

The SFE of the different substrates was calculated as a function of the contact angle hysteresis (CAH, H) with water (W), according to eqn (2) (ref. 28):

$$\gamma_S = \gamma_L(\cos\theta_r - \cos\theta_a)\{(1 + \cos\theta_a)^2/ [(1 + \cos\theta_r)^2 - (1 + \cos\theta_a)^2]\} \quad (2)$$

where γ_S is the surface free-energy of the solid (mN m^{-1}); γ_L is the surface tension of the test liquid (mN m^{-1}); θ_a is the advancing contact angle; and θ_r is the receding contact angle.

The Owens–Wendt method (OWM) was also used. This model splits the SFE into two components: the long-range dispersion, also named dispersive or non-polar (Lifshitz–van der Waals; γ_s^d), and the short-range polar (hydrogen bonding; γ_s^p) components of SFE according to eqn (2), thus providing more detailed information for the surfaces studied:[29]

$$W_{SL} = (1 + \cos\theta)\gamma_L = 2(\gamma_s^d)^{1/2}(\gamma_L^d)^{1/2} + 2(\gamma_s^p)^{1/2}(\gamma_L^p)^{1/2} \quad (3)$$

where W_{SL} is the work of adhesion at the solid–liquid interface; γ_L is the surface tension of the test liquid (mN m^{-1}); $\gamma_L{}^d$ is the dispersive component of the test liquid; $\gamma_L{}^p$ is the polar component of the test liquid; and γ_s is the SFE of the surface (mN m^{-1}).

The two components of the SFE for the recombinamer substrates were determined from the average values for the advancing contact angle of a non-polar liquid, in this case *n*-tetradecane (T, Sigma Aldrich), and deionized water (W). The values of the surface tension (γ) as well as the dispersive (γ^d) and polar (γ^p) components of the surface tension for these two test liquids are (in mN m^{-1}): $\gamma_T = 26.56$, $\gamma_T{}^d = 26.56$, and $\gamma_T{}^p \approx 0$, and $\gamma_W = 72.8$, $\gamma_W{}^d = 21.8$, and $\gamma_W{}^p = 51$.

The interfacial free energy (IFE; γ_{SW}) between water and the different recombinamer substrates was calculated from the surface free-energies of water and the surfaces according to eqn (4): (ref. 29)

$$\gamma_{SW} = \gamma_S + \gamma_W - 2(\gamma_S^d\gamma_W^d)^{1/2} - 2(\gamma_S^p\gamma_W^p)^{1/2} \quad (4)$$

Cell culture assays

Cell culture. Human Primary Fibroblasts HFF-1 (ATCC, USA) were maintained in DMEM with GlutaMAX™-I (Invitrogen), supplemented with 15% fetal bovine serum (FBS) (GIBCO) and penicillin/streptomycin (100 U mL^{-1}/100 μg mL^{-1}; GIBCO), at 37 °C in a humidified atmosphere comprising of 5% CO_2 and 95% air. The medium was changed every three days during the experiment. Cell passages 4–7 were used in all cell experiments.

HFF-1 cells were seeded at a density of 10^4 cells per cm^2 on surfaces placed on 12-well culture plates after a short trypsin/EDTA treatment. The total metabolic activity of the cells on the different surfaces analyzed was checked by measuring the fluorimetric reduction of alamarBlue® (AbD Serotec). Briefly, the seeded substrates were incubated for 4 hours with fresh culture medium supplemented with 10 vol% alamarBlue®. Following incubation, 100 μL of the medium from each well was transferred to a 96-well polystyrene microplate in triplicate. Fluorescence (excitation: 560 nm; emission: 590 nm) was measured using a SpectraMax M5e (Molecular Devices) microplate reader. Reduction of alamarBlue® by the cells, expressed as fluorescence emission intensity units, was measured at regular time intervals over a period of three weeks. A viability calculation was performed as per protocol and control cell values normalized to 100% viability. Three independent experiments, each one in triplicate, were performed for all substrates.

Cell behavior after early adhesion. HFF-1 cells suspended in serum-free medium were seeded at a density of 10^4 cells per cm^2 on surfaces placed on 12-well plates after a short trypsin/EDTA treatment. Loosely adhered or unbound cells were removed by changing the surfaces to a new plate 30 min after seeding and then maintained for seven days, changing the medium every three days.

Cell morphology was examined by SEM at 4 h and immunofluorescence staining at 4 and 24 h. The number of cells during the period of the experiment was quantified using the LIVE/DEAD® Viability/Cytoxicity Assay Kit (Molecular Probes) at 24 h and 5 and 7 days. Three independent experiments, each one in triplicate, were performed for all substrates.

Immunofluorescence staining. The cells were fixed for 10 min in a 4% paraformaldehyde solution and then permeabilized by exposure to a 0.5% Triton X-100 in PBS/0.1% BSA solution. The samples were then incubated overnight at 4 °C with a 1 : 280 dilution of the primary antibody (monoclonal anti-vinculin from mouse; Sigma) and then with a 1 : 200 dilution of the secondary antibody (Alexa Fluor 568 rabbit anti-mouse; Invitrogen) for an additional 5 hours at room temperature. F-actin was stained with Alexa Fluor 488 phalloidin (Molecular Probes) and the nuclei with 4′,6-diamino-2-phenylindole (DAPI) (Lonza). All staining steps were followed by an extensive washing with PBS/0.1% BSA solution. Finally, cell inspection was performed under a fluorescent inverted microscope (NIKON Eclipse Ti) and cell captures were made using the NIS Elements BR software (version 3.05).

Statistical analysis. A parametric one-way analysis of variance (ANOVA) was used to evaluate the data with *post-hoc* differences between groups using Bonferroni's corrected *t*-test with GraphPad Prism 4.0. A *p*-value of less than 0.05 was considered to be statistically significant. Results are shown as mean ± standard deviation (SD).

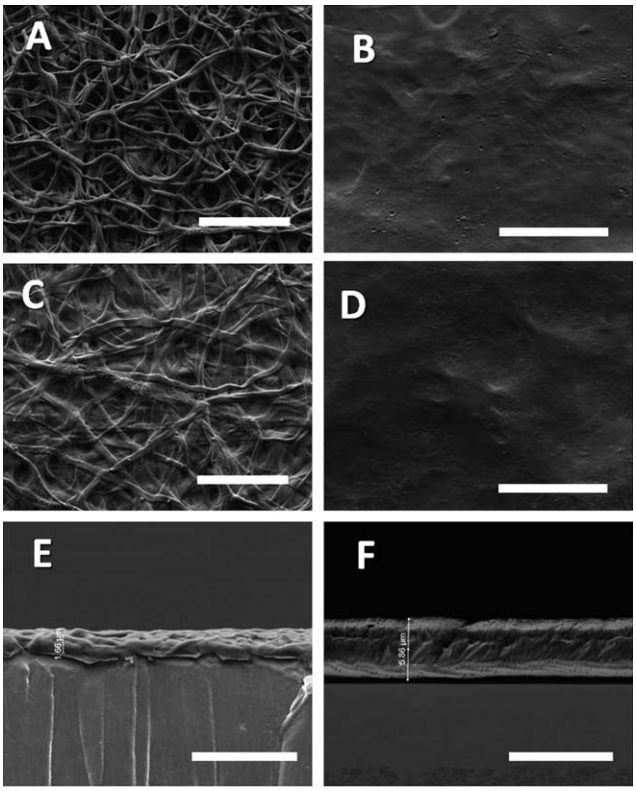

Fig. 1 SEM images of RGD6 ELR fibers (A), RGD6 films (B), IK24 fibers (C), IK24 films (D), and profile views of fibers (E) and films (F). Scale bar 20 μm in (A–D) and 10 μm in (E) and (F).

Results and discussion

Surface chemistry

The recombinamers used in this work are the biofunctionalized ELR known as RGD6 and the control IK24. RGD6 contains six equally spaced units of the fibronectin-derived RGD domain along the recombinamer chain, which represent the primary integrin-binding sequence and the amino acids that maintain the optimal conformation for interacting with integrins. These cell-binding domains are escorted by VPGIG/VPGKG pentapeptide block repeats that confer elastomeric properties on the resulting polymer and cross-linking through lysine residues. The control and non-biofunctionalized polymer (IK24) consists of the same isoleucine and lysine elastin-like pentapeptide block repeats as the RGD6 polymer but lacks the fibronectin-derived RGD domain. The detailed amino-acid sequences of the ELRs used are depicted below:

RGD6: $\{[(VPGIG)_2(VPGKG)(VPGIG)_2]_2AVTG\mathbf{RGD}SPASS[(VPGIG)_2\ (VPGKG)(VPGIG)_2]_2\}_6$

IK24: $[(VPGIG)_2(VPGKG)(VPGIG)_2]_{24}$

To successfully ensure the expected properties of the bio-produced recombinamers, their purity, monodisperse character, M_w, and NMR spectra were first checked, as reported previously.[15] The dissimilarities in their composition resulting from the inclusion of adhesion domains produced negligible differences in the thermoresponsive behavior of those recombinamers (Table 1).

As a fibrous structure is common to most ECMs, the possibility to mimic such a structure is of particular interest for tissue engineering applications. The multiple benefits arising from an ability to produce fibers based solely on tailored elastin recombinamers have been underexploited and have not been previously compared with other topographical conformations.

In this work, the experimental processing variables that determine the shape and the size of the electrospun fibers were investigated to obtain continuous and uniform fibers lacking beads or other defects. The fibers formed under the conditions described above showed a ribbon-like appearance and were randomly and isotropically distributed over the entire surface (Fig. 1A–C). No statistically significant differences in the diameters of the RGD6- (869 ± 226 nm) and IK24-based fibers (892 ± 325 nm) were found. Indeed, these diameters are of a scale where cells can sense them as individual fibers.[25] Fiber deposition on surfaces was programmed such that a mass of polymer equal to that obtained for the polymeric films formed by solvent casting was deposited per unit area (~4 mg of polymer per cm^2). Recombinamers in the form of films gave rise to almost flat layers (Fig. 1B–D). Both types of topographies were analyzed by SEM to determine their profiles and surface homogeneity. The thickness of the solvent-cast films (around 5–6 μm) and electrospun fibers (around 1.5 and 2 μm) guaranteed their homogeneity and complete coverage of the substrates on which they were deposited (Fig. 1E–F).

XPS monitoring of the chemical changes on the surfaces was focused on analysis of the disappearance of distinctive elements on the supports employed for recombinamer deposition and the concomitant emergence of elements characteristic of this deposition (Table 2). The latter were evidenced by the emergence of an N1s peak, which is specific for the recombinamers but not present for the supports, for both kinds of surface. Likewise, the decrease in the percentage oxygen content and the disappearance

Table 2 XPS results for the surfaces covered by ELRs in their different conformations and their corresponding supports. Data represent the percentage of the element atomic concentrations. Dashes represent values below the detection limit of this technique

	Elements											
Surfaces	C1s	N1s	O1s	Si2p	P2p	Na1s	Mg2s	K2s	Ti2p	Zn2p3	In3d5	Sn3d
Glass	12.10	0.23	41.81	29.70	1.41	2.05	8.60	2.75	0.58	0.80	—	—
RGD6 films	78.69	8.96	12.02	—	—	—	—	—	—	—	—	—
IK24 films	76.13	10.15	12.32	1.41	—	—	—	—	—	—	—	—
ITO	46.94	—	31.13	20.73	1.20	—	—	—	—	—	20.73	1.20
RGD6 fibers	70.06	16.91	13.03	—	—	—	—	—	—	—	—	—
IK24 fibers	74.20	11.71	14.08	—	—	—	—	—	—	—	—	—

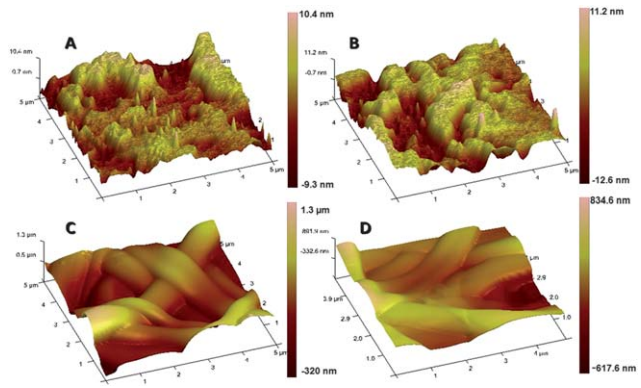

Fig. 2 AFM images of (A) RGD6 films, (B) IK24 films, (C) RGD6 fibers, and (D) IK24 fibers.

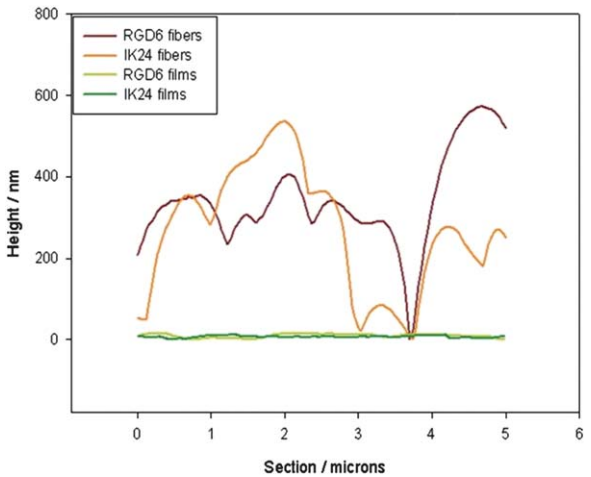

Fig. 3 Roughness scaled profiles from four random sections of the surfaces under study.

of In3d5 and Sn3d for ITO, and Si2p for glass also confirmed the total coverage of the support by the recombinamers.

Surface topography

The topographical features of the ELR surfaces were studied by AFM in tapping mode (Fig. 2). In order to make a more suitable comparison of the surface properties, Fig. 3 combines the profiles of four random sections of the different topographical samples studied, on the same height scale, in a single graph, thus highlighting the greater surface area to volume ratio of the fibers with respect to the films. The RMS values contained in Table 3 were calculated from these AFM images with the same dimensions (5×5 µm). Although these AFM captures appear to suggest that the films (micrographs in Fig. 2A and B) have rougher surfaces than the fibers (Fig. 2C and D), it should be noted that the image scales for the fibers and films differ by two orders of magnitude. Thus, as roughness is scale-dependent and differences can appear depending on the area studied, the roughness values for fibers and films obtained from these captures should not be compared. In this sense, both fibers and films have a similar roughness for the different recombinamers, with the RGD topographies being slightly rougher than their IK24 counterparts.

Thereafter, the comparison between fibers and films with respect to higher roughness can be interpreted in terms of a larger specific surface.

Surface free energy

Surface free-energy (SFE; γ_s) is one of the most commonly used parameters for quantifying the quality of a material's surface and its potential applications.[1,30] Most methods used to calculate the SFE of solids use contact angle measurements. Contact angle hysteresis (CAH; H) exists when there is an inequality between the advancing, or wetting, angle (θ_a) and the receding, or dewetting, angle (θ_r), and its value is obtained by subtracting both terms.[31] The difference between advancing and receding contact angles of water (H) is a good means of evaluating the physical roughness and/or chemical heterogeneity of surfaces.[32–34] Thus, the lower the adhesion of a liquid droplet to the solid, the lower the contact angle hysteresis and the easier it is for the droplet to flow along the surface.[35] A syringe pump was used when measuring the advancing and receding contact angles in order to advance or remove the test liquids at a constant rate. In the case of the advancing contact angle, the constant addition of water makes the drop expand, thereby increasing the liquid–solid interfacial area. This can be thought of as the "wetting angle" as the drop can now wet an additional area. This situation is reversed in the case of the receding contact angle, and the "dewetting angle" is measured when fluid is withdrawn. As absorption of water by the ELR structures is unavoidable, as can be deduced by the greater hysteresis found between the polymer-coated surfaces when compared with the smoother surfaces used as supports, both dynamic contact angles were measured in the stable phase of advance or recoil on both sides of the drop by adding or withdrawing sufficient test liquid for each measurement. The H values obtained in our work were in good agreement with both RMS roughness and SFE distribution. As deduced from the experimental data (Table 3), there is a direct relationship between the surface topography (in terms of RMS

Table 3 Data collected from contact angle measurements and AFM analysis (all surface tension components are in mN m^{-1}). The values obtained on glass and ITO have been included for comparative purposes

Surfaces	RMS (SD)/nm	θ_a (SD) (T)	θ_a (SD) (W)	θ_r (SD) (W)	H (W)	γ_s^p	γ_s^d	$\gamma_{s\ (OWM)}$	$\gamma_{s\ (CAH)}$	γ_{SW}
RGD6 fibers	371.30 (143.60)	29.31 (4.81)	84.12 (5.95)	17.05 (4.31)	67.07	2.46	23.20	25.66	28.80	31.08
RGD6 films	3.08 (2.83)	43.75 (3.77)	50.77 (7.60)	15.29 (8.77)	35.48	29.29	19.63	48.92	53.88	3.05
IK24 fibers	336.70 (68.81)	29.27 (4.51)	73.36 (7.95)	20.30 (1.81)	53.06	11.74	23.21	34.95	37.22	13.82
IK24 films	2.78 (1.25)	39.70 (2.73)	48.94 (4.80)	18.23 (4.48)	30.71	30.04	20.79	50.83	55.57	2.77
Glass	0.18 (0.03)	22.96 (2.03)	60.40 (3.74)	33.90 (4.57)	26.50	19.03	24.46	43.49	41.58	7.79
ITO	1.40 (0.11)	27.79 (1.63)	111.03 (0.58)	84.32 (0.93)	26.71	0.01	23.47	23.48	17.15	49.61

roughness) and hysteresis shown by the contact angle. Thus, the greater the roughness of the surface of the material, the greater the hysteresis shown by the contact angle on it. In other words, water droplets adhere better to fiber surfaces than to films. This is probably due to the enhanced interfacial area of fibers with respect to films, which means that surface forces become dominant as the surface area-to-volume ratio increases. This increase in the surface prevailing effect was corroborated by SFE calculations as being a function of the contact angle hysteresis. The SFE calculated on the basis of the contact angle (θ) measures the non-covalent forces between a liquid and the first monolayer of the material and can thus be deduced from eqn (2). The results of these calculations showed a higher SFE for film surfaces than for fiber surfaces (Table 3). The SFE values obtained by this method showed a similar trend to those obtained using the Owens–Wendt method (OWM), with higher SFEs for smoother surfaces.

Several substrate properties, including surface charge, topography, hydrophobicity or hydrophilicity, surface chemistry and surface energy, have been proposed to influence cell behavior in culture. It is generally accepted nowadays that the adhesion and spreading of cells on polymer surfaces are related to the polar and dispersion components of the SFE.[36] In accordance with the OWM, the SFE can be divided into two terms where γ_d represents the dispersive component and γ_p the polar component of the surface energy, as illustrated in eqn (3). When non-polar test liquids, such as *n*-alkanes, are used as adsorbates, the polar term becomes zero and the work of adhesion is dominated by dispersive interactions at the interface; the calculated surface energy components of the surface are then used to give a quantitative determination of the magnitude of their hydrophobicity. Recombinamers in the form of films have a larger SFE, with a higher polar component and lower dispersive component, than fibers, where the dispersive component predominates. Therefore, as the chemical composition of the two different sets of recombinamers is the same, the SFE differences must be attributable to the conformation induced by the different topographies. However, it should be noted that the differences shown by the polar components in the two fiber substrates (9.6% of the SFE for RGD6 and 33.6% for IK24) do not correspond to the small differences found for the polar components of the two recombinamer substrates in the form of films (59.9% for RGD6 and 59.1% for IK24).

Surface energy aspects are usually regarded as being fundamental to an understanding of adhesion, with the surface energy of a substrate determining the degree of wetting or spreading of any material at their interface. However, in adhesion science and technology, it is common to gloss over the formal distinction between the concepts of surface tension and surface energy and to refer to them both as "surface energy" and "surface free energy" (SFE). Although both concepts are expressed in the same units (*per unit area*), surface tension (γ) and surface energy (γ_{SW}) exhibit subtle differences in formal treatments. Thus, surface tension refers to the intermolecular forces that hold a material together. In other words, in the bulk of a material, each molecule is surrounded on all sides by other molecules, thus meaning that the forces between them balance out, the entire mass is in equilibrium and the work required to create a new surface defines surface tension. On the other hand, the surface energy term strictly describes the unbalancing excess of energy associated with the presence of a surface, in other words the interfacial forces associated with the presence of a surface.[37]

Cell adhesion is a very complicated process that is traditionally considered to involve at least four major steps prior to proliferation, namely protein adsorption, cell–substrate contact, cell–substrate attachment, and cell spreading. As the protein-adsorption step involves molecular-scale interactions with the substrate in the presence of the aqueous culture medium, the surface properties of substrates may have an important influence on the conformation of proteins and on the competition between their adsorption at interfaces.[38] When determining cell behavior on solid surfaces, it has been suggested that the interfacial free energy (IFE; γ_{SW}) between the culture medium and the substrates is a more appropriate parameter for describing surface properties rather than the SFE.[39] These interfacial interactions may provide clues regarding how cells grow on specific substrates. The IFE between water and ELR surfaces under study was calculated according to eqn (4) to analyze the differences in the IFE between substrates and to attribute them to different cellular behaviors, if any, in a subsequent comparative cellular study. The results (Table 3) suggest that the contribution of each system to the free energy due to the presence of an interface (IFE) was higher for the fibrous supports than for films, with the former showing up to a 10 times higher excess surface energy than the latter.

Likewise, the differences between fibers as a result of their constituent ELRs were more pronounced. The presence of the RGD sequence provided a more pronounced energetic excess on fibers, whereas this difference between the two kinds of films was negligible.

The adsorption of molecules at interfaces to decrease the free energy of the system is a thermodynamically driven process, and it has been proposed that a direct proportionality exists between the IFE and the adsorption capacity at an interface.[40] Most of the culture media employed are supplemented with nutrients that compete, to a greater or lesser degree, depending on the substrate, for adsorption onto the materials where they are dispensed, particularly as regards wettability and the electrical properties of the surface. In addition, adsorption of proteins onto the material surfaces involves conformational rearrangements that, in the case of hydrophobic surfaces, could cause the initial adsorbed protein layer to denature.[39,41] To determine whether such phenomena could have affected the energy results obtained, and whether a direct proportionality exists between the IFE and the capacity for adsorption at an interface, a comparative study of cell behavior on each of the previously characterized surfaces was carried out.

Cell behavior assays

Although the biocompatibility of cross-linked fibrous elastin structures has been demonstrated previously,[11,17] differences in cell behavior when influenced simultaneously by both topographical cues and bioactivity, as derived from the presence of cell adhesion domains, have not been reported previously. In our work, cell proliferation was confirmed by quantifying the total metabolic activity of cells, and by vital and immunochemical staining in both short- and long-term studies.

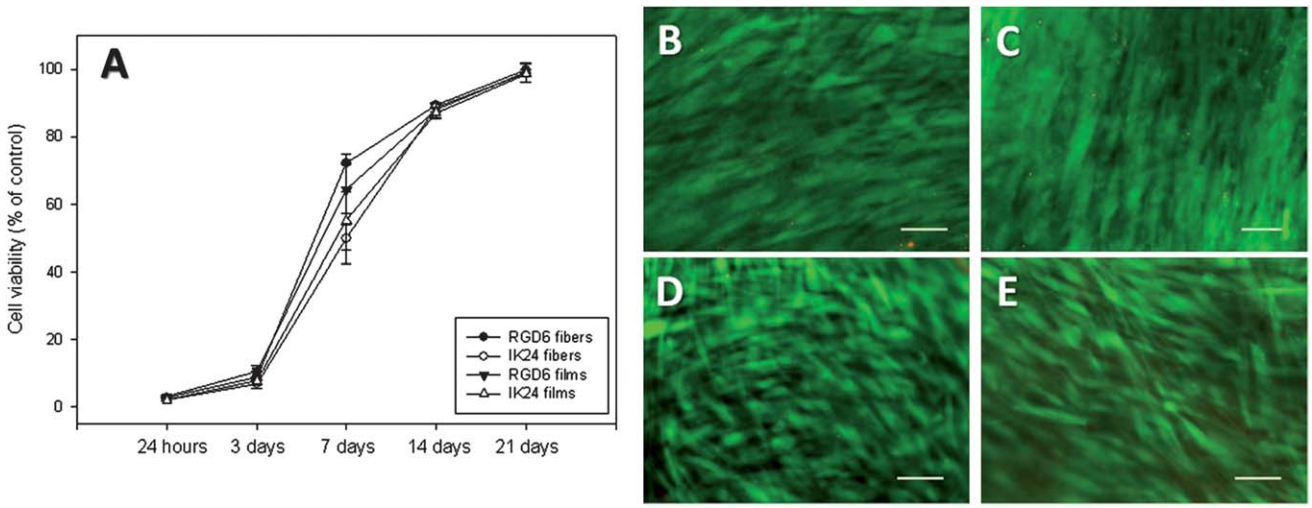

Fig. 4 Cell viability of HFF-1 fibroblasts grown during 21 days using the optimized alamarBlue reduction assay (A). LIVE and DEAD differential staining of the HFF-1 cells following 21 days of culture on RGD6 fibers (B); IK24 fibers (C); RGD6 films (D); and IK24 films (E). Scale bar: 50 μm.

In an initial long-term proliferative experiment, human fibroblasts were grown for three weeks on the different surfaces. Cell growth was found to increase with total cellular activity on all the surfaces studied, with almost 100% viability at the end of the period tested (Fig. 4).

However, although no significant differences were found in the cell proliferations at any time point ($p > 0.05$), RGD6 surfaces always supported higher proliferation rates than their non-bioactive equivalents, irrespective of the topography, with the greatest differences being detected in the initial stages and during the exponential growth stage (especially at $t = 7$ days). For this reason, the numerical and morphological differences during the early phases of adhesion, and the cell fate up to day 7, were analyzed in a more detailed manner.

A second experiment, in which loosely adhered or unbound cells were removed from the surfaces after 30 min of incubation, was performed in order to determine the cell fate as a function of the extent of initial attachment to the different surfaces (Fig. 5).

The quantitative analysis showed that the presence of RGD motifs was the main factor controlling early cell adhesion for both topographies. Thus, as can be seen from Fig. 5A, at 24 hours the RGD surfaces clearly retained the largest numbers of adhered cells, with a high level of significance when compared with their corresponding non-functionalized counterparts ($p < 0.001$). In contrast, no significant differences ($p > 0.05$) were found between the surfaces of IK24, where only a few cells were found after seeding and rinsing. Further studies showed a slightly, but significantly, higher cell-adhesion rate as regards RGD6 films than RGD6 fibers ($p < 0.05$) and a higher level of dead cells on non-biofunctionalized fibers than on all other surfaces.

The differences between surfaces became more noticeable at longer culture times. Thus, at day 5, except for RGD6 substrates ($p > 0.05$), significant differences were found amongst all surfaces ($p < 0.001$), although the difference between RGD6 fibers and IK24 films was somewhat less significant ($p < 0.05$). These differences were subsequently maintained and, in some cases, increased. Thus, at day 7, an increase in the significance of the different cell growth between RGD6 fibers and RGD6 films ($p < 0.001$), and between RGD6 fibers and IK24 films ($p < 0.001$),

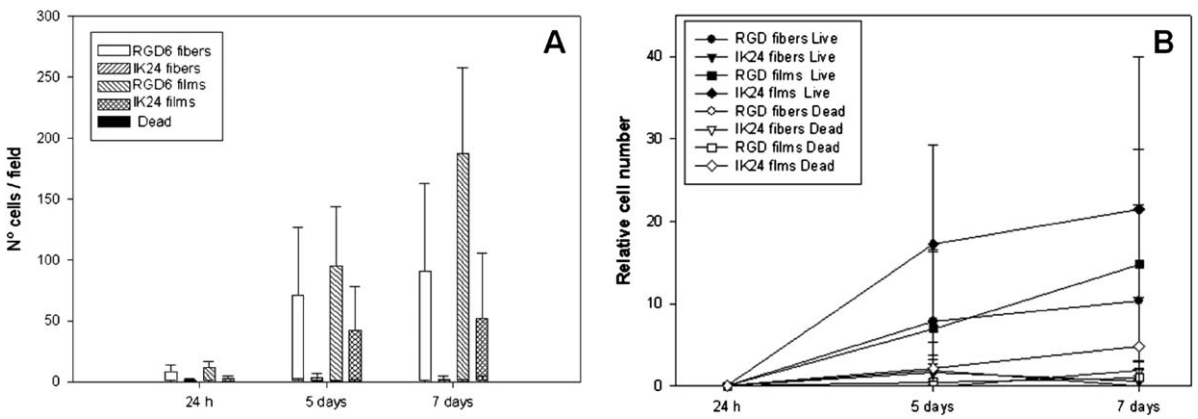

Fig. 5 Proliferation of HFF-1 cells on the different recombinamer surfaces. (A) Average number of cells at 24 h and 5 and 7 days in the field of view when using the 10× objective after cell staining. The average is obtained by analyzing nine random sites on each surface, in triplicate. (B) Values of the relative increase in cell number, at the same time points as in the previous section, with respect to the initial cell number (at 24 h) for each experiment. See text for significance analysis.

was found. In summary, it can be seen that the presence of adhesion sequences on the functionalized surfaces promotes a more rapid growth than in controls in the same time period, thus meaning that such surfaces showed more cells per unit area after day 7. This behavior could be affected by the fact that, during the initial stages, the number of cells found on supports with better adhesion properties is higher than that found on less adherent substrates, for which the first rinsing stage drastically reduces the cell number. Thus, to avoid this potential artifact, the results obtained from the absolute cell counts were normalized with respect to the initial cell number. The results of this analysis are summarized in Fig. 5B.

Surprisingly, proliferation on IK24 films increased 21.5-fold after 7 days, the highest proliferation rate of all surfaces tested. In contrast, cells on IK24 fibers were barely able to grow and proliferate, remaining at levels close to zero after 7 days of culture. RGD6 films and fibers increased their initial cell loads 14.7- and 10.3-fold, respectively. These results suggest three clearly differing trends: the IK24 film group, with high proliferation rates despite low initial adhesion; the RGD group (both fibers and films), with good initial adhesion and proliferation rates; and the IK24 fibers group, with neither of these previous two properties. All these results are related and are consistent with the hydrophilicity and the IFE of the surfaces tested. Higher proliferation rates were obtained on the most hydrophilic substrates and those with the lowest IFE with water, in other words the polymeric films. It is noticeable that, although they contain similar polar components, IK24 films were slightly more hydrophilic than their RGD6 analogs, thus suggesting that the higher proliferative capacity of cells over highly hydrophilic surfaces is probably more closely related to the surface properties than to the presence of bioactivity, although, as can be deduced from the absolute numbers of cells, the latter is a synergic factor. In contrast, as can be deduced from the almost complete lack of cells on IK24 fibers compared with the apparently normal proliferative rate seen on RGD6 fibers, bioactivity acquires much higher relevance for energetically unfavorable surfaces.

Differences in proliferation rates are usually accompanied by morphological changes to the cell. Indeed, the cellular response to an adherent surface is usually manifested by an increase in cell spreading, the activation of survival signaling pathways, and the activation of focal adhesion assembly.[42]

The response of human fibroblasts to ELR-coated surfaces at 4 h post-seeding caused evident cell spreading over the surfaces of those substrates containing RGD sequences, whereas the absence of RGDs restricted normal cell spreading for both types of topographies. SEM images taken at this time (Fig. 6) only showed a fine cell-based film on the different bioactive surfaces.

In addition, cells on RGD fibers spread in an elongated fashion, whereas on RGD films they adopted a more regular and isotropic shape. However, small, spherical, perfectly visible, and apparently unattached cells were the dominant trend on the non-bioactive surfaces. Cell immunostaining corroborated the SEM results and provided new information regarding the focal adhesion assembly. Thus, vinculin was present in a diffuse form around the perinuclear region and/or as discrete focal adhesions that differed according to the surface (Fig. 7). Thus, spindle shapes with large protrusions in all directions around the cells were found in cells seeded on RGD6 fibers. These cellular

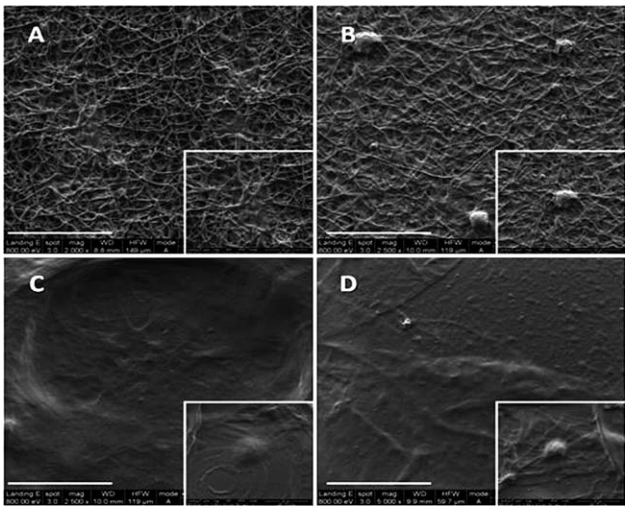

Fig. 6 Low-vacuum SEM captures of HFF-1 cells at 4 hours post-seeding. (A) RGD6 fibers, (B) IK24 fibers, (C) RGD6 films, and (D) IK24 films. Scale bars for larger figures: 50 μm. Scale bar for insets: 20 μm.

extensions revealed vinculin clustering of activated integrins, as can be inferred from the red coloration of all these structures, which, in addition, were numerous and not restricted to the cell

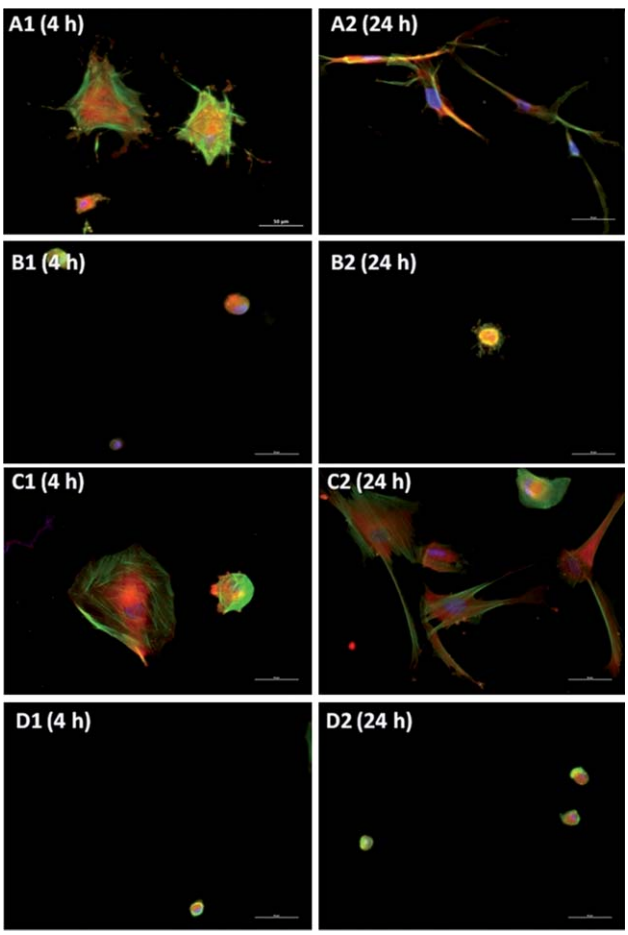

Fig. 7 Immunostaining of actin (green), vinculin (red), and nuclei with DAPI (blue) of HFF-1 cells cultured for 4 h and 24 h on RGD6 fibers (A), IK24 fibers (B), RGD6 films (C), and IK24 films (D). Scale bars: 50 μm.

periphery. This intense projection in the response of the cells to the presence of adhesion motifs was reflected in the arrangement of actin fibers, which adopted a relatively chaotic organization consistent with the massive formation of adhesive structures after integrin activation. On the other hand, cell spreading on the RGD6 films was rather more regular in terms of cell shape, focal adhesion assembly, and actin filament distribution. Focal adhesion was intense in the perinuclear area, as in the case of fibers, but showed more regular spacing and smaller projections, resembling a rounded cell morphology, at the periphery. In addition, the actin cytoskeleton was more pronounced and regular than in the case of RGD6 fibers. Changes in actin organization tended to progressively adapt the cells to the topography of the substrates, as can be seen from subsequent immunostained captures on RGD substrates. HFF-1 cells exhibited an increased elongation on fibers at 24 h, whereas a slight additional elongation could be seen on films made of the same polymer at the same time. The apparent lack of cell response to non-functionalized surfaces remained after 24 hours post-seeding.

Cell morphology and viability after short-term contact with the substrates were analyzed at 24 h and 5 and 7 days in order to evaluate whether the former has some effect on the latter. As can be seen from Fig. 8, fewer morphological differences were observed as the number of cells increased, with increasingly standard fibroblastic shapes being formed on all surfaces except

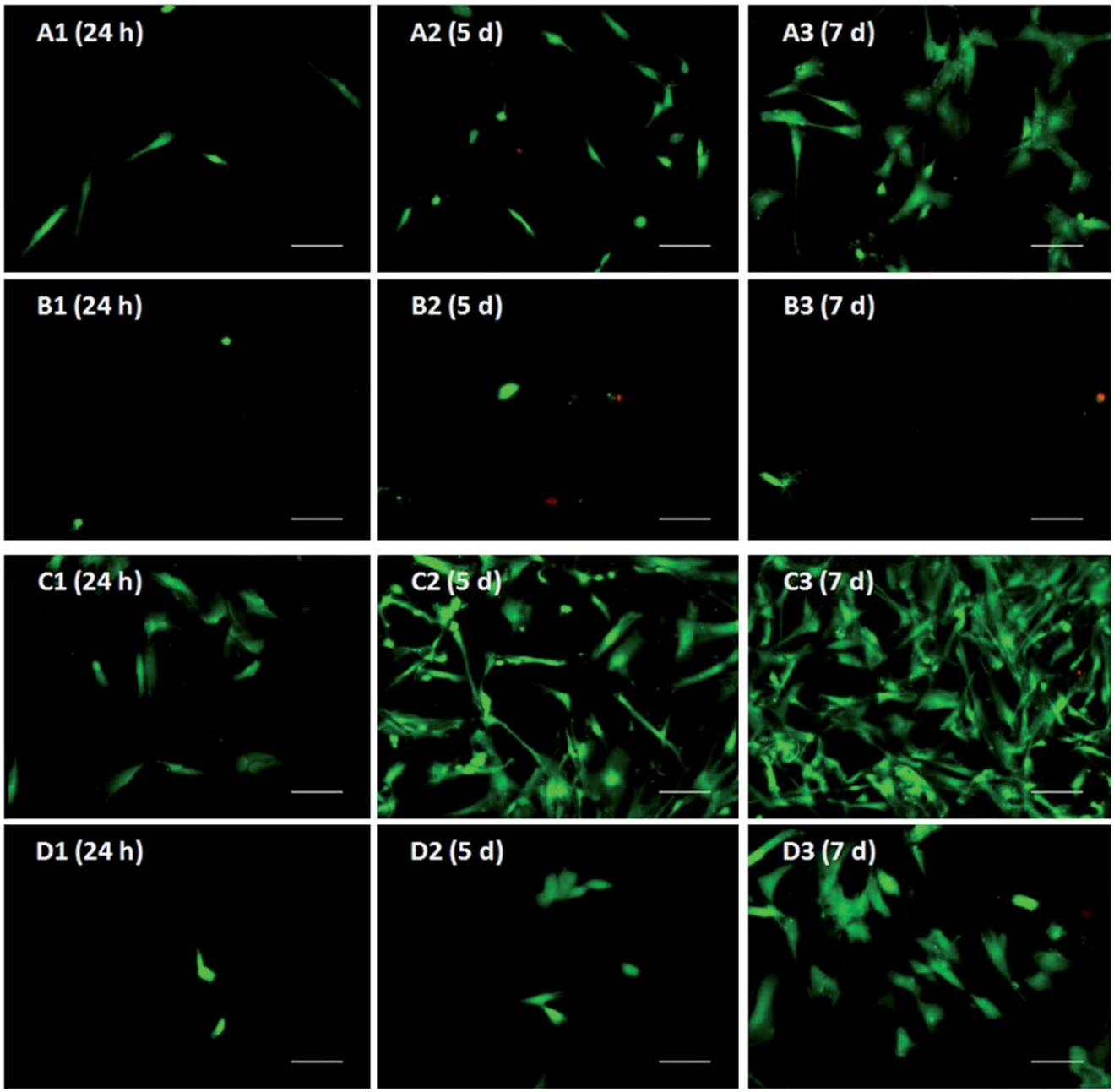

Fig. 8 Morphological analysis of the cells at 24 hours (24 h), 5 days (5 d), and 7 days (7 d) after adhesion on RGD6 fibers (A), IK24 fibers (B), RGD6 films (C), and IK24 films (D). Scale bar: 100 μm.

for IK24 fibers, where cells were unable to grow. Thus, cells on fibers tended to have less elongated profiles during the initial stages of adhesion, whereas on films they tended to adopt the peculiar fibroblast fusiform elongation observed on standard supports rather than the more circular form observed initially. The cellular morphologies produced by the topographies did not affect the viability or the final cell counts.

Although surface hydrophobicity is known to affect protein adsorption, its effect on cell behavior remains controversial in the light of inconsistent experimental data.[43,44] The adhesion of mammalian cells to a material is mediated mainly by the presence of a protein adlayer, which in turn depends on the substrate, particularly its wettability and the electrical properties of its surface, and on the composition of the liquid phase. A competition between proteins that inhibit (such as serum albumin) and those that promote cell adhesion (such as fibronectin), together with substrate-dependent changes in the conformation of adsorbed serum proteins, could be responsible for modulating integrin binding and proliferation of cells on non-intrinsically bioactive surfaces with high IFEs.[33] This could explain why, on pretreated albumin surfaces and in the presence of serum factors in the culture medium (needed to support cell growth), proteins tend to be adsorbed to a larger extent onto materials with a higher IFE (fibrous ones) which, in turn, could inhibit cell adhesion and hinder surface–cell interactions. Such an effect could prevent cell adhesion and proliferation on IK24 fibers and promote a lower growth on RGD6 fibers than on RGD6 films. In the case of the RGD6 structures, two beneficial conditions, namely a lower IFE between the culture medium and the substrate and the presence of adhesion motifs, come together to overcome the advantage of higher exposure of RGD assumed for the fiber form under the same conditions. In the case of IK24 films, the high long-term proliferation rates despite low initial adhesion could be overcome by beneficial surface energy conditions.

Conclusions

The incorporation of functional groups into polymers to modify their surface without changing the bulk properties of the material is especially important in those biomaterials where specific interactions between the surface and cells are required. Due to the key role that proteins play in cell–cell and cell–matrix interactions, this goal is easily achievable with ELRs.

The two topographies obtained from each of the ELRs used in this work modify the surface properties of their supporting materials in a fast and easy manner and provide very different surface properties in terms of wettability. These differences affect the morphological and proliferative responses of cells seeded on them to a marked degree.

The higher IFE of the fibers with respect to films probably increases the thermodynamic driving force for the greater adsorption of proteins from the aqueous culture medium, thereby hindering cell–surface interactions.

The high cell densities found in the long-term assays demonstrate the biocompatibility and suitability of ELRs in both topographies for tissue engineering applications, whereas the short-term contact of cells with the different substrates conditioned the morphological and proliferative cell fate. The highest proliferation rates were obtained on the most hydrophilic substrates and those with the lowest IFE. These values were also enhanced by the inclusion of specific adhesion sequences. The energetically unfavorable environment for cell growth found in the most hydrophobic substrates was counteracted by inclusion of the specific adhesion motifs described for the previous topography.

The higher proliferative capacity of cells over highly energetic surfaces (in terms of SFE) is probably more closely related to the surface properties than to the presence of bioactivity, although the latter could be a boosting factor that acts in the early stages of culture. However, the bioactivity acquires much greater significance for energetically unfavorable surfaces by ensuring cell adhesion and subsequent proliferation.

Acknowledgements

We acknowledge financial support from the EU through the European Regional Development Fund (ERDF), from the MICINN (projects MAT 2007-66275-C02-01, MAT 2009-14195-C03-03, MAT-2010-15982, and MAT2010-15310), the JCyL (projects VA034A09 and VA030A08), the CIBER-BBN (project CB06-01-0003), and the JCyL and the Instituto de Salud Carlos III under the "Network Center of Regenerative Medicine and Cellular Therapy of Castilla and León".

References

1 J. Skopinska-Wisniewska, A. Sionkowska, A. Kaminska, A. Kaznica, R. Jachimiak and T. Drewa, *Appl. Surf. Sci.*, 2009, **255**, 8286–8292.
2 J. L. Dalsin and P. B. Messersmith, *Mater. Today*, 2005, **8**, 38–46.
3 A. Folch and M. Toner, *Biotechnol. Prog.*, 1998, **14**, 388–392.
4 M. Arnold, E. A. Cavalcanti-Adam, R. Glass, J. Blümmel, W. Eck, M. Kantlehner, H. Kessler and J. P. Spatz, *ChemPhysChem*, 2004, **5**, 383–388.
5 R. A. Kriparamanan, P. Aswath, A. Zhou, L. Tang and K. T. Nguyen, *J. Nanosci. Nanotechnol.*, 2006, **6**, 1905–1919.
6 K. von der Mark, J. Park, S. Bauer and P. Schmuki, *Cell Tissue Res.*, 2010, **339**, 131–153.
7 M. Tirrell, E. Kokkoli and M. Biesalski, *Surf. Sci.*, 2002, **500**, 61–83.
8 V. Beachley and X. Wen, *Prog. Polym. Sci.*, 2010, **35**, 868–892.
9 R. Vasita and D. S. Katti, *Int. J. Nanomed.*, 2006, **1**, 15–30.
10 T. J. Sill and H. A. von Recum, *Biomaterials*, 2008, **29**, 1989–2006.
11 W. F. Daamen, J. H. Veerkamp, J. C. M. van Hest and T. H. van Kuppevelt, *Biomaterials*, 2007, **28**, 4378–4398.
12 J. C. Rodríguez-Cabello, L. Martín, M. Alonso, F. J. Arias and A. M. Testera, *Polymer*, 2009, **50**, 5159–5169.
13 J. C. Rodríguez-Cabello, L. Martín, A. Girotti, C. García-Arévalo, F. J. Arias and M. Alonso, *Nanomedicine*, 2011, **6**, 111–122.
14 A. Ribeiro, F. J. Arias, J. Reguera, M. Alonso and J. C. Rodriguez-Cabello, *Biophys. J.*, 2009, **97**, 312–320.
15 R. R. Costa, C. A. Custodio, A. M. Testera, F. J. Arias, J. C. Rodriguez-Cabello, N. M. Alves and J. F. Mano, *Adv. Funct. Mater.*, 2009, **19**, 3210–3218.
16 H. Martinez-Osorio, M. Juarez-Campo, Y. Diebold, A. Girotti, M. Alonso, F. J. Arias, J. C. Rodriguez-Cabello, C. Garcia-Vazquez and M. Calonge, *Curr. Eye Res.*, 2009, **34**, 48–56.
17 L. Nivison-Smith, J. Rnjak and A. S. Weiss, *Acta Biomater.*, 2010, **6**, 354–359.
18 M. R. Dreher, A. J. Simnick, K. Fischer, R. J. Smith, A. Patel, M. Schmidt and A. Chilkoti, *J. Am. Chem. Soc.*, 2008, **130**, 687–694.
19 J. Andrew MacKay, M. Chen, J. R. McDaniel, W. Liu, A. J. Simnick and A. Chilkoti, *Nat. Mater.*, 2009, **8**, 993–999.
20 L. Martin, M. Alonso, M. Moller, J. C. Rodriguez-Cabello and P. Mela, *Soft Matter*, 2009, **5**, 1591–1593.
21 L. Huang, R. A. McMillan, R. P. Apkarian, B. Pourdeyhimi, V. P. Conticello and E. L. Chaikof, *Macromolecules*, 2000, **33**, 2989–2997.

22 M. Li, M. J. Mondrinos, M. R. Gandhi, F. K. Ko, A. S. Weiss and P. I. Lelkes, *Biomaterials*, 2005, **26**, 5999–6008.
23 J. C. Liu and D. A. Tirrell, *Biomacromolecules*, 2008, **9**, 2984–2988.
24 M. L. Carman, T. G. Estes, A. W. Feinberg, J. F. Schumacher, W. Wilkerson, L. H. Wilson, M. E. Callow, J. A. Callow and A. B. Brennan, *Biofouling*, 2006, **22**, 11–21.
25 D. T. Mcpherson, C. Morrow, D. S. Minehan, J. G. Wu, E. Hunter and D. W. Urry, *Biotechnol. Prog.*, 1992, **8**, 347–352.
26 J. C. Rodríguez-Cabello, A. Girotti, A. Ribeiro and F. J. Arias, *Methods Mol. Biol.*, 2012, **811**, 17–38.
27 A. Girotti, J. Reguera, F. J. Arias, M. Alonso, A. M. Testera and J. C. Rodríguez-Cabello, *Macromolecules*, 2004, **37**, 3396–3400.
28 M. Żenkiewicz, *JAMME*, 2007, **24**, 137–145.
29 D. K. Owens and R. C. Wendt, *J. Appl. Polym. Sci.*, 1969, **13**, 1741–1747.
30 C. S. Chen, M. Mrksich, S. Huang, G. M. Whitesides and D. E. Ingber, *Science*, 1997, **276**, 1425–1428.
31 R. S. Faibish, W. Yoshida and Y. Cohen, *J. Colloid Interface Sci.*, 2002, **256**, 341–350.
32 P. G. Degenes, *Rev. Mod. Phys.*, 1985, **57**, 827–863.
33 T. S. Chow, *J. Phys.: Condens. Matter*, 1998, **27**, L445–L451.
34 G. Zografi and S. S. Tam, *J. Pharm. Sci.*, 1976, **65**, 1145–1149.
35 M. Nosonovsky, *Langmuir*, 2007, **23**, 3157–3161.
36 E. M. Harnett, J. Alderman and T. Wood, *Colloids Surf., B*, 2007, **55**, 90–97.
37 D. E. Packham, *Int. J. Adhes. Adhes.*, 2003, **23**, 437–448.
38 M. Ni, W. H. Tong, D. Choudhury, N. A. A. Rahim, C. Iliescu and H. Yu, *Int. J. Mol. Sci.*, 2009, **10**, 5411–5441.
39 A. Carré and V. Lacarrière, in *Contact Angle, Wettability and Adhesion*, ed. K. L. Mittal, VSP/Brill, Leiden, Netherlands, 2008, vol. 5, pp. 253.
40 E. H. Lucassen-Reynders, *J. Phys. Chem.*, 1963, **67**, 969–972.
41 B. G. Keselowsky, D. M. Collard and A. J. García, *J. Biomed. Mater. Res., Part A*, 2003, **66**, 247–259.
42 B. Geiger, J. P. Spatz and A. D. Bershadsky, *Nat. Rev. Mol. Cell Biol.*, 2009, **10**, 21–33.
43 Z. Ma, Z. Mao and C. Gao, *Colloids Surf., B*, 2007, **60**, 137–157.
44 E. J. Chang, H. H. Kim, J. E. Huh, I. A. Kim, J. S. Ko, C. P. Chung and H. Man Kim, *Exp. Cell Res.*, 2005, **1**, 197–206.